ELSEVIER

Contents lists available at ScienceDirect

## Journal of Physics and Chemistry of Solids

journal homepage: www.elsevier.com/locate/jpcs





# Synthesis of Egyptian Blue and mechanisms

Agoston Kiss<sup>a</sup>, Holly A. Stretz<sup>a,\*</sup>, Akira Ueda<sup>b</sup>, Richard Mu<sup>c</sup>

- <sup>a</sup> Department of Chemical Engineering, Tennessee Technological University, PO Box 5013, 1020 Stadium Drive, Cookeville, TN, 38505, USA
- <sup>b</sup> Department of Life and Physical Sciences, Fisk University, 1000 17th Avenue North, Nashville, TN, 37208, USA
- c TSU Interdisciplinary Graduate Engineering Research Institute, Tennessee State University, 3500 John A. Merritt Boulevard, Nashville, TN, 37209, USA

## ARTICLEINFO

Keywords:
Sensors
IR fluorescence
TGA-MS
High temperature XRD
Cuprorivaite

#### ABSTRACT

Egyptian Blue (EB, Cuprorivaite,  $CaCuSi_4O_{10}$ ) is a novel candidate for nanomaterial-based sensors in water, as its infrared (IR, 910 nm) emission has high quantum yield in comparison with current commonly-used IR reporters. IR signals for bioimaging and environmental sensing penetrate biological matrices (i.e. tissues) deeper and with less scattering than visible light. This work reports the effects of heating rate on the solid state synthetic yield of EB and formation mechanism is discussed. EB synthesis was investigated with thermogravimetric analysis coupled with mass spectrometry and *in-situ* high temperature X-ray diffraction. A reproducible maximum in EB yield was observed at a heating rate of 7 °C/min with samples containing CaCO<sub>3</sub> precursor. We report the optimized reaction conditions, yields, and the photoluminescent response of the synthesized EB layered materials. The precursor content (O<sub>2</sub>, CaCO<sub>3</sub>, CuO and SiO<sub>2</sub>) also had a subtle effect on EB yield.

## 1. Introduction

Near-infrared (NIR) optical imaging has been given a considerable amount of attention in the past decade, especially in biomedical applications [1-5], but the library of nanoscale probes has been somewhat limited. The family of 2-D layered materials useful for optical devices is even more restricted [6]. Single wall nanotubes, quantum dots, semiconducting polymers and small molecule organic dyes such as indocyanine dye are among these probes [7], none of which join the exciting new layered materials that are 2-D. An ancient pigment, Egyptian Blue (EB, CaCuSi<sub>4</sub>O<sub>10</sub>) or cuprorivaite, a 2-D nanoparticulate material, has received an increasing amount of attention recently in such applications due to its very high quantum yield ( $\Phi = 10.5\%$ ) and long luminescence lifetime (107 µs) [8]. EB was first synthesized around 3100 B.C. in Egypt [9-11] for decorative purposes and is only very recently being investigated as an active nanomaterial in optical sensors [1-5] and microwave emitters [12] due to its intense near-infrared (NIR) emission at 910 nm [13]. Several methods of EB synthesis have been explored [14-21], however the mechanism of the synthesis, factors affecting the purity and control of uniformity of the product have been reported only sporadically. The synthesis mechanism, factors affecting the purity of the product, and better understanding of control of uniformity of the product size and shape are needed to engineer a uniform coating of EB nanoparticles to enable its use in sensing. Uniform, nano-sized particles

of EB will be needed to ensure the performance of the sensor's coating. EB is generally formed in a high temperature solid synthesis, where control of nanoparticle size is less understood. Borisov et al. [1] reported a ball milling process during which they obtained microparticles (1–5  $\mu$ m) of EB though these are not small enough for many applications in nanotechnology such as bioimaging [3–5] and latent fingermark detection [22]. Borisov et al. did not report the uniformity of these EB particles. Johnson-McDaniel et al. [20] reported a hydrothermal formation method for EB, in which they produced 40–60  $\mu$ m crystals with uniform, flowerlike morphology. In their particle size distribution analysis, the most frequent particles were between 45 and 55  $\mu$ m. The traditional salt-flux method [23] and solid-state synthesis [19] can also be used to produce EB, however neither route provides control over product morphology or size [20].

Johnson-McDaniel et al. [19] reported a melt flux, as well as a solid-state synthesis, where they reacted CaCO<sub>3</sub>, CuO and SiO<sub>2</sub> in a 1:1:4 M ratio, respectively, at 1020 °C for 16 h to obtain EB, compared to 72 h for the hydrothermal process described by Johnson-McDaniel [20]. The morphology of EB samples made with the melt flux and solid-state methods were compared with transmission electron microscopy (TEM). The TEM images showed that the lateral dimensions of EB particles ranged from hundreds of nanometers to several microns. The EB sample made with the solid-state method had rougher edges, which suggested a more heterogeneous composition compared to the EB with a

<sup>\*</sup> Corresponding author. 1020 Stadium Drive, Prescott Hall Room 214, Cookeville, TN, 38505, USA.

E-mail addresses: akiss42@tntech.edu (A. Kiss), hstretz@tntech.edu (H.A. Stretz), aueda@fisk.edu (A. Ueda), rmu@tnstate.edu (R. Mu).

more homogeneous surface produced with the melt flux. A more homogeneous surface (distinct platelets) suggested a better quality of EB [20].

Current commonly used infrared reporters [24,25] for fluorescent emission have luminescence quantum yields of  $\Phi = 0.00014$ –0.47%. EB has at least an order of magnitude greater luminescence quantum yield ( $\Phi = 10.5$ %) and a long luminescence lifetime (107 µs) [8]. This extremely high luminescence quantum yield and long emission lifetime makes EB a potential candidate for a fluorescent emission analysis in applications such as the biomedical or environmental fields (bioimaging of neurotransmitters and pathogens) [3–5], silica based optical amplifiers [26–28], laser technology [29], and microwave emitters [12].

Understanding the formation mechanism of solid-state synthesized EB layered materials will lead to improved control of yields and potential control of uniformity of morphology. Solid-state synthesis requires extreme temperatures (~1000 °C), and heating rate should be explored as possibly affecting yield. Thermogravimetric analysis (TGA) coupled with mass spectrometry (MS) and high-temperature X-ray diffraction (HT-XRD) were used for the exploration of such reaction mechanisms as related to yield, when heating rate was the independent variable

### 2. Materials and methods

#### 2.1. Materials

Two mixtures were tested, both of which have been reported in the literature [17,19] as synthetic starting materials in solid-state synthesis.

## 2.1.1. Mixture 1

A reaction mixture of CaCO<sub>3</sub> (99.98%, Mallinckrodt), CuO (98%, Aldrich Chemical Company, Inc.) and amorphous SiO<sub>2</sub> (99.9%, CERAC, incorporated) (see Supplemental Information for XRD pattern, Fig. S15) was prepared in a 1:1:4 M ratio, respectively, with a mortar and pestle [19].

## 2.1.2. Mixture 2

A reaction mixture of CaO (99.95%, Thermo Fisher Scientific), CuO (98%, Aldrich Chemical Company, Inc.) and amorphous  $SiO_2$  (99.9%, CERAC, incorporated) was prepared in a 1:1:4 M ratio, respectively, with a mortar and pestle [17].

## 2.2. Synthesis using thermogravimetric analyzer (TGA)

The thermal syntheses were performed using a Thermogravimetric Analyzer (TGA, Discovery) coupled with a quadrupole mass spectrometer (MS, Discovery) at the Polymer Characterization Lab at The University of Tennessee, Knoxville. Five fresh samples of bulk Mixtures 1 and 2 were heated in a ceramic pan in the TGA. The temperature ranged from 23 °C to 1050 °C with five different heating rates of 5, 6, 7, 8, and 10 °C/min in air. The samples were held isothermally at 1050 °C for 5 min at the end of the scan opposed to the suggested very long reaction times, such as 16 h, reported by Johnson-McDaniel [19].

Ion currents were measured continuously for m/z 1–300 AMU with the MS. The ion currents belonging to m/z of nitrogen (14, 28, and 29 (isotopic) AMU), oxygen (16, 18 (isotopic), and 32 AMU), and argon (40 AMU) (air contains argon) were removed from scans presented here and largely attributed to interference by carrier gas composition. In later sections Si (m/z = 28 AMU) and isotopic Si (m/z = 29 AMU) might have been expected to show up in the gas stream but the size in N<sub>2</sub> peak (also m/z = 28 AMU) and isotopic N<sub>2</sub> peak (also m/z = 29 AMU) would make it difficult to de-complex. Si will show up as other species if present, such as SiO radical [30–32].

## 2.3. Characterization using X-ray diffraction (XRD)

X-ray diffraction (XRD) analysis was performed using a Rigaku Ultima IV diffractometer. A normal line focus  $CuK_{\alpha}$  radiation tube was used with power settings of 40 kV, 44 mA. Measurements were made using a D/teX Ultra High-Speed Detector with the detector discriminator set in a fluorescent reduction mode. All samples for a given processing condition were loaded into an automatic rotary sample changer, and diffraction patterns were recorded using a scan speed of  $2.00^{\circ}$ /min and a scan range from 10.0 to  $70.0^{\circ}$  20. The raw data were imported into the PDXL: Integrated X-ray powder diffraction software package for phase analysis. These were then compared with the standard patterns in the International Center for Diffraction Data (ICDD) database.

## 2.4. Thermal synthesis using X-ray diffraction

Five fresh samples of bulk reaction Mixtures 1 and 2 were heated in the Rigaku XRD instrument from 23 °C to 1050 °C with five different heating rates of 5, 6, 7, 8, and 10 °C/min in dry air atmosphere (30 mL/min). XRD patterns were obtained at the starting temperature (23 °C), then at every 100 °C until 1000 °C, at 1020 °C, 1050 °C, 1050 °C after 5 min isothermal, and finally at 23 °C again once cooled off. This temperature profile mirrored that of the TGA experiments. In some cases, a surface layer was formed during the scan (to be discussed more in depth later). Each sample was then separately homogenized with a mortar and pestle, and then rescanned in the XRD instrument at constant temperature of 23 °C. The yields were calculated by the software using the Reference Intensity Ratio (RIR) method [33].

# 2.5. Scanning Electron Microscopy (SEM) and Energy Dispersive Spectroscopy (EDS)

A Hitachi Ultra-High-Resolution Schottky Scanning Electron Microscope (SEM) SU7000 with a ZrO/W Schottky Emitter, operated at 5 kV was used to determine the morphology of the synthesized EB samples. Energy Dispersive Spectroscopy (EDS) data were collected with an Octane Elect EDS system, using the APEX™ software. The samples were prepared for SEM by putting fragments of the synthesized EB on a carbon tape. The samples were not coated with any metallic element.

## 2.6. Fluorescence spectroscopy

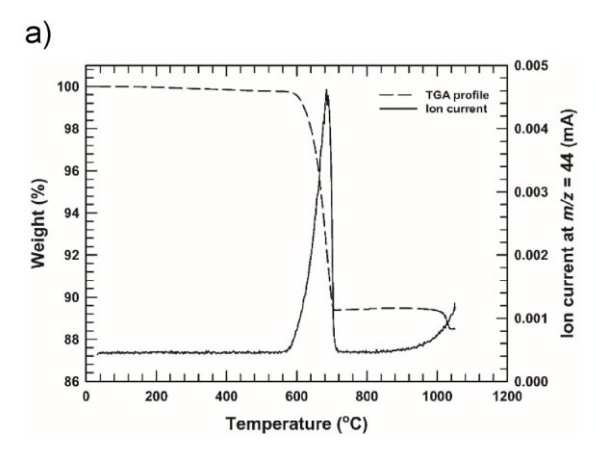
Fluorescence spectroscopy was carried out on a Horiba Scientific Lab RAM HR 800 instrument with a CCD detector at Fisk University in Nashville, TN. The laser (532.14 nm wavelength) used was a Ventus (diode-pumped solid-state laser) from Laser Quantum.

## 3. Results and discussion

## 3.1. Thermogravimetric analysis results

The samples were analyzed initially for evidence of off-gas production using TGA coupled with MS. The reactions expected to produce a gas were:  $\text{CaCO}_3 \rightarrow \text{CaO} + \text{CO}_2$  [10]. Five fresh samples of Mixture 1 and Mixture 2 were heated in the TGA from 23 °C to 1050 °C with five different heating rates. Samples were not processed at higher temperatures because degradation has been reported above 1050 °C [15]. A representative TGA-MS scan of Mixture 1 (containing CaCO<sub>3</sub>) is shown in Fig. 1a.

Degradation events were observed at two temperature ranges, at 600-700 °C and at 1020-1025 °C. The 600-700 °C event might be explained as the decomposition of CaCO<sub>3</sub> to CaO [10]. The event at 1020-1025 °C is could be the evaporation of SiO<sub>2</sub> during the EB synthesis. SiO<sub>2</sub> is able to form volatile compounds (mainly SiO, with m/z=44) at high temperatures and low O<sub>2</sub> partial pressures and evaporate into the annealing atmosphere [30-32]. Similar TGA profiles were



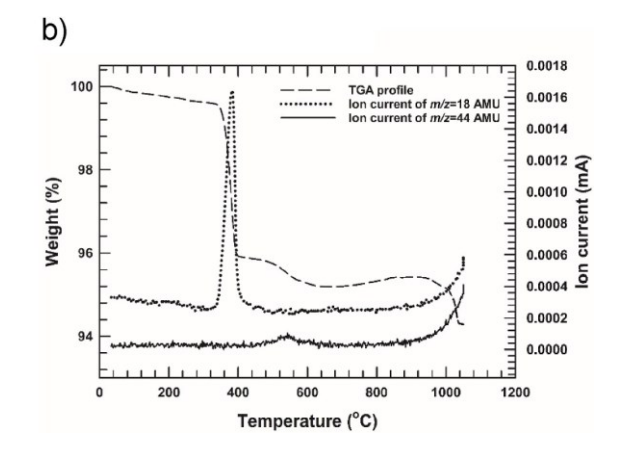


Fig. 1. a) TGA (dashed line) coupled with MS (solid line) profile of EB synthesis with a heating rate of  $7 \,^{\circ}$ C/min in air, starting with CaCO<sub>3</sub>. TGA off gas was recorded in MS at ion current of m/z = 44 AMU (CO<sub>2</sub>). CO<sub>2</sub> was lost with maximum at 685  $^{\circ}$ C. b) TGA (dashed line) coupled with MS (dotted and solid lines) profile of EB synthesis with a heating rate of  $7 \,^{\circ}$ C/min starting with CaO in air.

obtained with the five different heating rates, supporting that the heating rate had no effect in this early analysis (see Figs. S16–19). The ion current curve will be discussed in section 3.2.

A TGA-MS scan of Mixture 2 (containing CaO) with a heating rate of 7  $^{\circ}$ C/min is shown in Fig. 1b.

This coupled analysis can confirm the hypothesis of  $CO_2$  production and  $SiO_2$  volatile compound formation. Decomposition events were observed at two temperature ranges, between 340 – 400 °C and 970–1000 °C. The first event is attributed to the decomposition of Ca (OH)<sub>2</sub> (e.g. CaO exposed to environmental moisture) to CaO [34]. The second event is attributed to the evaporation of  $SiO_2$  during the EB synthesis. Note that the synthesis with Mixture 2 (containing CaO) occurred at a lower temperature than with Mixture 1 (containing  $CaCO_3$ ).

## 3.2. Mass spectrometry (MS)

TGA off-gas was analyzed with a coupled MS. There was a large peak in the ion current belonging to m/z = 44 AMU between 600 and 700 °C for Mixture 1, with a maximum at 685 °C. This is attributed to off-gas of  $CO_2$  from decomposition of  $CaCO_3$  in air and has been documented by Wiedemann and Berke [10]. The areas under the ion current curves with different heating rates were determined (Table 1).

From the increase in area, we conclude that the amount of evolving CO<sub>2</sub> increased with the heating rate. This observation had implications for the yield in Mixture 1 if it was a result of the CaCO<sub>3</sub> not converting completely to CaO at lower heating rates and if CaO was a necessary reactant to produce EB.

An increase in the same ion current (m/z = 44 AMU) was observed as the temperature reached the 1020-1025 °C range, possibly due to the  $SiO_2$  evaporating in the form of SiO from the sample. Another peak was observed in the ion current belonging to m/z = 12 AMU between 600 and 700 °C for Mixture 1. The peak belonging to the m/z = 12 AMU was attributed to the carbon ion fragment originating from the  $CO_2$ .

The ion currents of m/z = 18 AMU vs temperature were compared for

Table 1 Integrated areas under the MS ion current curves (m/z = 44 AMU, CO<sub>2</sub> production) with different heating rates.

Heating rate (°C/min)	Area (unit)
5	0.1502
6	0.1924
7	0.2224
8	0.2324
10	0.2888

Mixtures 1 and 2 (Figs. S3 and S10, respectively). No significant jumps were observed in the ion current of m/z = 18 for Mixture 1 at any temperatures. This suggested that Mixture 1 did not contain detectable amounts of water (m/z = 18 AMU). Therefore, the small ion current of m/z = 18 AMU for Mixture 1 was attributed to isotopic oxygen. A large peak was detected in the same ion current for Mixture 2 between 340 and 400 °C, which was attributed to water loss due to the decomposition of Ca(OH)<sub>2</sub> to CaO [34]. A representative mass spectrum is shown for the EB synthesis at 1020 °C starting with CaCO<sub>3</sub> in Fig. 2a.

The ion currents belonging to m/z = 17, 20, 34, and 44 AMU were found to be significant at 1020 °C. The m/z = 44 AMU was attributed to SiO radical. The ion currents of m/z = 17, 20, and 34 AMU were plotted versus the entire temperature range, however no significant jumps were observed in these ion current profiles. A mass spectrum is shown for the EB synthesis at 1020 °C starting with CaO in Fig. 2b.

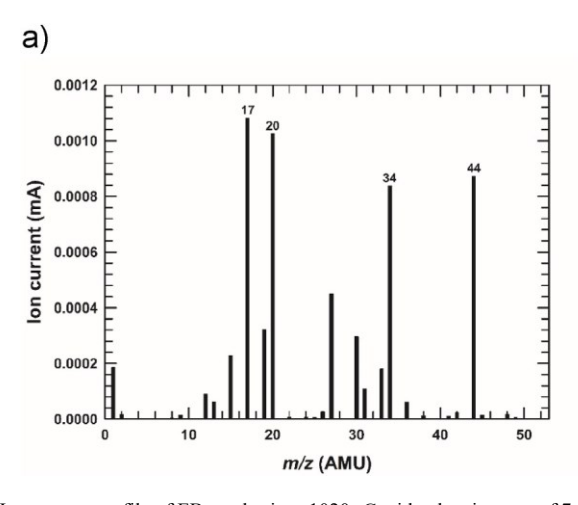
The ion currents belonging to m/z = 20, 27, 34 and 44 AMU were found to be significant at 1020 °C. The m/z = 44 AMU was again attributed to SiO radicals. The ion currents of m/z = 20, 27, and 34 AMU were plotted versus the entire temperature range; however, no significant jumps were observed in these ion current profiles. The volatile nature of SiO<sub>2</sub> at elevated temperatures such as 1020 °C is a very interesting observation and can be confirmed by other scientific sources [30–32].

## 3.3. Thermal synthesis using X-ray diffraction

High temperature XRD synthesis of EB was performed as a complement to the TGA-MS data to better understand the phases formed and lost during the synthesis. A representative scan of Mixture 1 (containing CaCO<sub>3</sub>) with a heating rate of 7 °C/min is shown in Fig. 3a.

The scan at 23 °C confirmed the presence of the starting materials: CaCO<sub>3</sub> (CC) and CuO (CU). The SiO<sub>2</sub> was not detected by the instrument, presumably due to its initial amorphous nature. The scan at 800 °C did not show detectable CaCO<sub>3</sub> peaks; instead CaO (CA) peaks appeared at this temperature. The scan at 1050 °C showed that there were Ca<sub>2</sub>CuO<sub>3</sub> (D), CuO (CU), high quartz (Q), and cristobalite (S) in the system. Similar XRD patterns with different relative peak intensities were observed for all heating rates.

The resulting powders formed in the XRD temperature scans exhibited two visibly different layers. The top layer, which was in contact with air, had a grey color. The bottom layer, which was in contact with the sample holder, had a dark blue color. The top layer was separated manually and rescanned in the XRD instrument at room temperature. The XRD results indicated that the top layer contained unreacted CuO, Ca<sub>2</sub>CuO<sub>3</sub>, and alpha-quartz (SiO<sub>2</sub>). No EB was measured. The bottom layer was scanned, as well, and the resulting XRD pattern



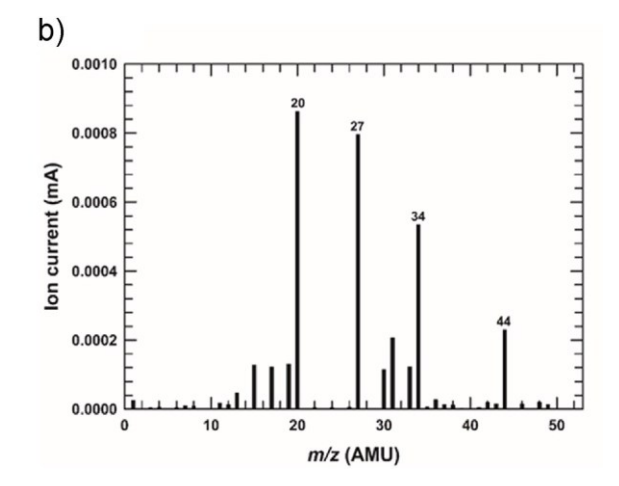
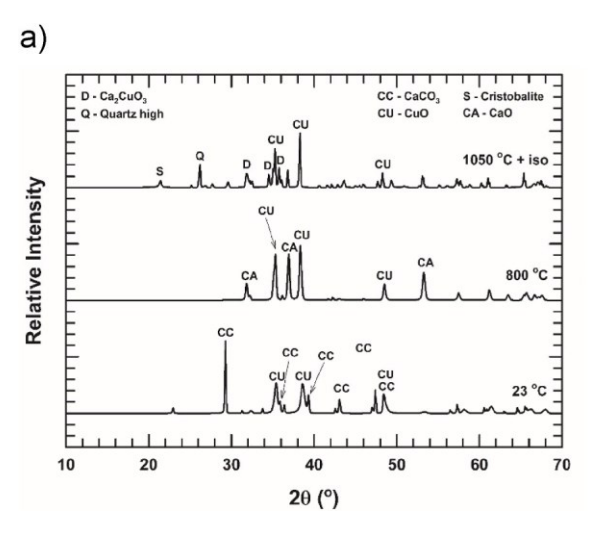


Fig. 2. a) Ion current profile of EB synthesis at 1020 °C with a heating rate of 7 °C/min. The sample contained CaCO<sub>3</sub> precursor. b) Ion current profile of EB synthesis at 1020 °C with a heating rate of 7 °C/min. The sample contained CaO precursor.



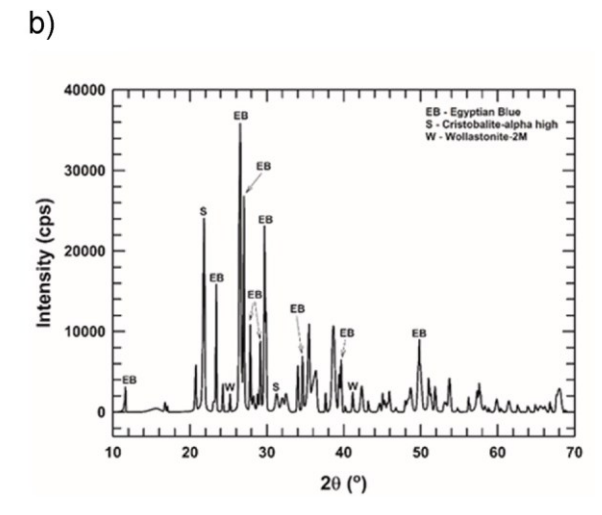


Fig. 3. a) XRD analysis for the top layer at points of thermal synthesis, ramped at 7 °C/min b) XRD pattern of EB synthesis with 7 °C/min heating rate. Main product is EB, with cristobalite-alpha high –  $SiO_2$  – (S), and wollastonite-2M –  $CaSiO_3$  – (W) unreacted materials.

confirmed the presence of EB (Fig. 3b) along with unreacted cristobalite (S) and wollastonite-2M (W).

For the yield calculations, each sample was homogenized to combine the two layers and then scanned in the XRD at room temperature. The yields (calculated with the RIR method) were plotted against the different heating rates (Fig. 4).

For error bar calculation 3 sets of samples were heated in the XRD, the yields were then normalized for each sample using the yield at  $7\,^{\circ}$ C/min (highest yield) and then all trial results plotted against the heating rates (Fig. 5). (Error bars represent the standard deviation relative to the mean for 3 replicates.)

Both graphs (Figs. 4 and 5) indicated a reproducible maximum in the yield around the 7 °C/min heating rate. Questions these findings raised include:

- 1. Is cristobalite necessary for EB formation? Cristobalite has a more open microstructure than quartz, which allows a better incorporation of various other elements into the crystal structure [35].
- 2. Is O<sub>2</sub> necessary to form EB?
  - 3. Is either CaCO<sub>3</sub> or CaO necessary to form EB?
  - 4. Is a passivating layer formed on the top of the samples that affects yield through mass or heat transfer effect?

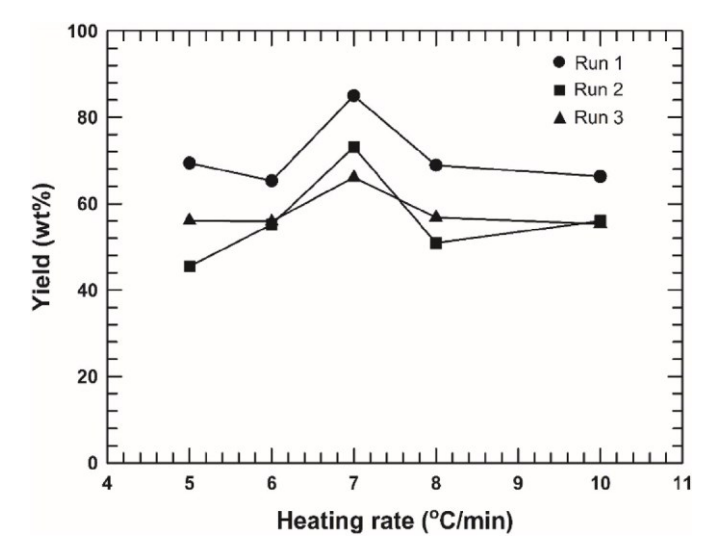


Fig. 4. First (●), second (■), and third (▲) set of EB samples with CaCO<sub>3</sub> precursor synthesized in XRD instrument.

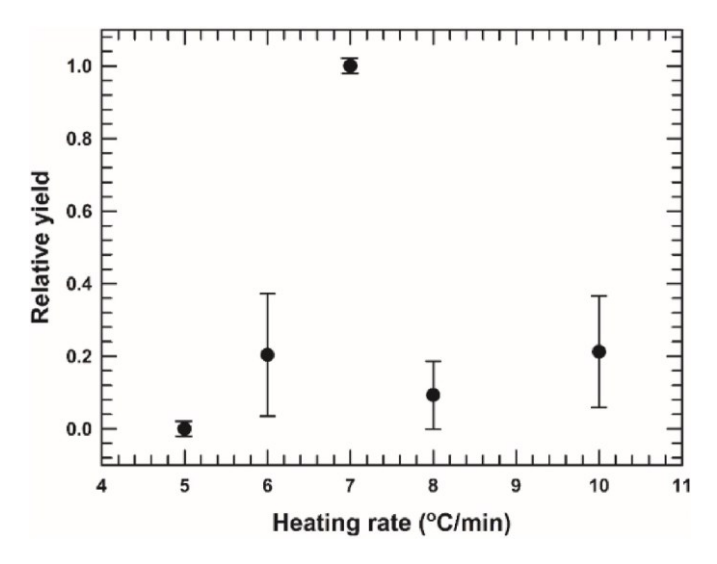


Fig. 5. Error bars calculated for the yields vs heating rates for 3 data points. Since data was normalized per run, highest and lowest values have no variance for this basis.

To address the first hypothesis, the percentages of cristobalite and EB, synthesized from Mixture 1 (containing CaCO<sub>3</sub>), in each homogenized and rescanned sample were calculated and plotted. No correlation was found between the percentages of cristobalite and EB. The space groups of cristobalite ( $P4_12_12$ ) [36] did not match the spacing of EB (P4/ncc) [23]. Therefore, cristobalite formation was not supported as an intermediate precursor to EB. It was also hypothesized that the phase transformation of the SiO<sub>2</sub> (conversion to tridymite and cristobalite at elevated temperatures) removed some SiO<sub>2</sub> of the quartz phase, vital to the formation of EB [18]. To assess this hypothesis, quantitative analysis (RIR) was performed on the XRD pattern of the samples at 1020 °C, 1050 °C, and 1050 °C + iso. No trend (e.g. increasing amount of tridymite/cristobalite with the increase of temperature) was found among the percentages of tridymite and cristobalite to confirm such a hypothesis.

Concerning the role of  $O_2$  in the synthesis, syntheses were also attempted in  $N_2$  atmosphere in the XRD ramped at 5, 6, and 7 °C/min. The CuO was reduced to Cu<sub>2</sub>O (Fig. 6) between 850 and 1000 °C and no EB peaks were detected.

When the sample was heated in N2 atmosphere, the O2 vapor

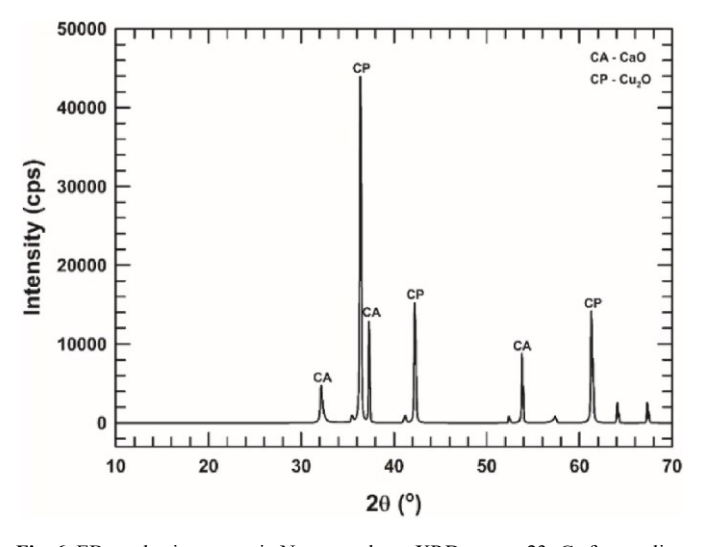


Fig. 6. EB synthesis attempt in  $N_2$  atmosphere. XRD scan at 23 °C after cooling from 1050 °C. Peaks belonging to EB and CuO were undetectable, the CuO was reduced to Cu<sub>2</sub>O.

pressure in the sample increased. If the upper layer was a barrier to byproduct diffusion,  $O_2$  could escape more readily through the porous upper layer at higher temperatures. As a result, the CuO could be reduced to  $Cu_2O$  in the mixture. No measurable EB forming in  $N_2$  atmosphere confirmed the hypothesis that  $O_2$  is needed for the formation of EB. This observation is consistent with the necessity of  $Cu^{2+}$  ions in the synthesis. If  $Cu^+$  ions are present, they do not support the formation of EB. When in a reducing atmosphere (e.g.  $N_2$ ) we hypothesize that  $Cu^+$  ions were formed, whereas in the presence of air they could not form.

Another research question was if either CaCO<sub>3</sub> or CaO was needed to form EB. Experiments were run with Mixture 2 (containing CaO) and EB formed (Fig. 7).

The yields with the CaO precursor were very close to the yields with the  $CaCO_3$  precursor (Fig. 4), however no correlation was found between the yield and the heating rate regarding the CaO samples. This indicated that both  $CaCO_3$  and CaO are good starting materials for the synthesis and produce similar yields of EB, but care must be taken with heating rate if  $CaCO_3$  is used as the precursor.

Reported solid-state syntheses generally require very long reaction times, such as 16 h, at elevated temperatures (e.g. 1050 °C) [19]. The samples analyzed for this paper were held at 1050 °C only for 5 min. Good yields (60–70%) of EB were still obtained (Figs. 4 and 7). The bottom part of the reaction mixture (in contact with the sample holder) was closer to the heating coils of the furnace. Due to the time limit and possible uneven distribution of heat, the grey upper layer, containing some unreacted starting materials (Figure 3a), perhaps represented a moving boundary as reaction proceeded.

### 3.4. Fluorescence spectroscopy

XRD gave evidence of EB formation in this solid-state synthesis, but to confirm its performance as a sensor, fluorescence emission of synthesized EB (in the HT-XRD with a heating rate of 7 °C/min) was also measured. The excitation wavelength was 532 nm in the spectrofluorometer. The strong fluorescent signal shown at 910 nm (Fig. 8) confirmed the presence of functional EB.

## 3.5. SEM-EDS

SEM-EDS was performed on the EB samples synthesized in the XRD (Fig. 9).

The calculated weight percentages of the O, Si, Cu, and Ca atoms in EB were 42.6%, 29.8%, 16.9%, and 10.7%, respectively. The sample

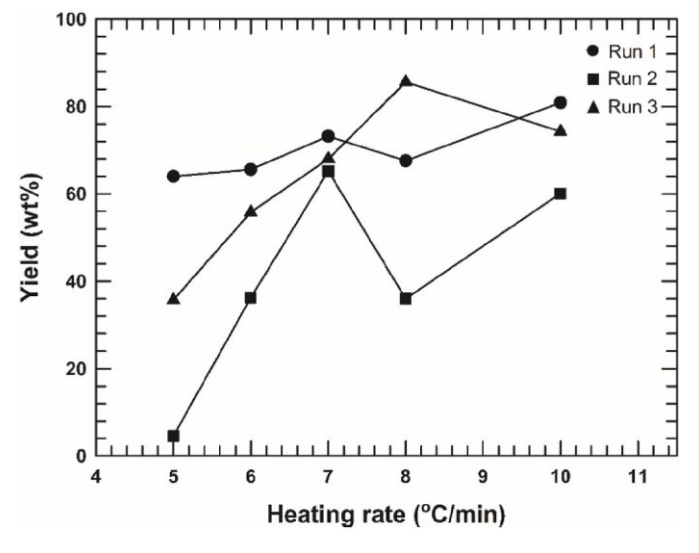


Fig. 7. First (lacktriangle), second (lacktriangle), and third (lacktriangle) set of EB samples with CaO precursor synthesized in XRD instrument.

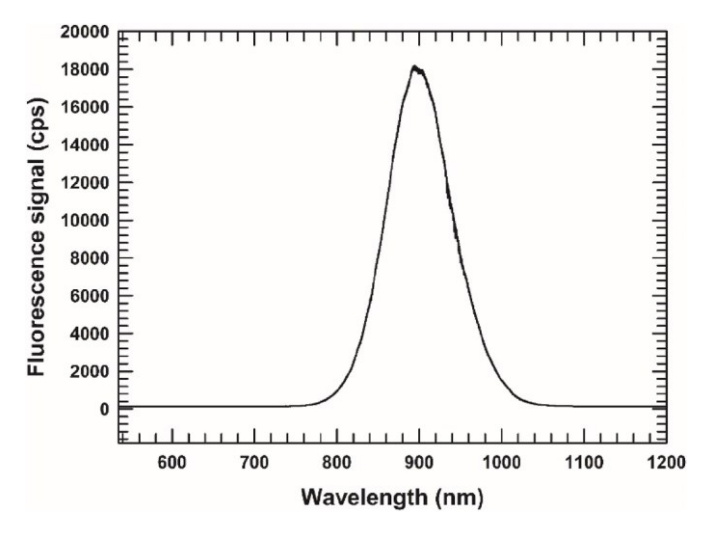


Fig. 8. Fluorescence emission of synthesized EB in the high temperature XRD with a heating rate of 7 °C/min. This fluorescent signal is characteristic of EB.

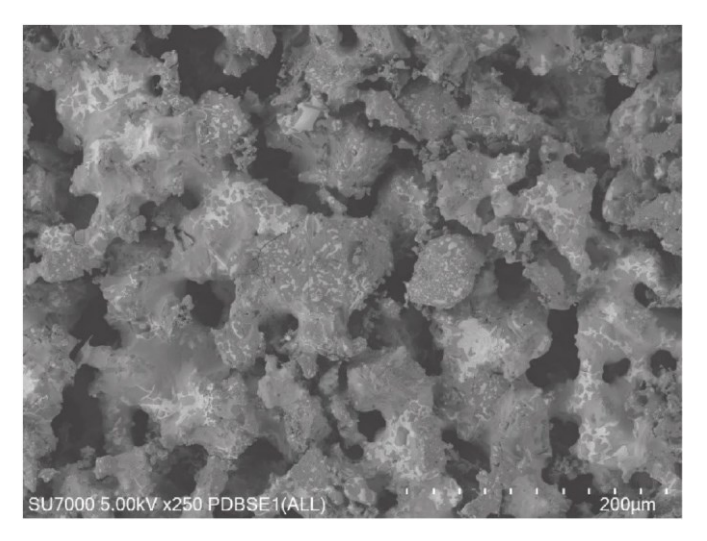


Fig. 9. SEM micrograph of synthesized EB.

analyzed (Fig. S20) contained 44.9% O, 32.0% Si, 13.0% Cu, 10.1% Ca. These measured weight percentages were very close to the calculated percentages of the respective atoms in EB, so the chemical composition of the sample matches that of the EB. The morphology of the synthesized EB samples looked very similar to the solid-state synthesis product reported by Johnson-McDaniel [19]. Our product did not exhibit flat 50  $\mu$ m surfaces that Johnson-McDaniel found in their melt flux synthesis. However, we found some of the smaller crystallite features of 1–15  $\mu$ m (Fig. 9). The controlled formation of particular shapes or sizes of EB particles is beyond the scope of these early studies, but will be explored in future work.

## 4. Conclusions

Egyptian Blue (cuprorivaite) is an inorganic 2-D layered material which fluoresces with extremely high quantum yield in the near IR. Important utility in the burgeoning arena of materials for novel optical devices in bioimaging and environmental sensing has been reported. The solid-state reaction mechanism of EB was explored through TGA-MS and HT-XRD analyses. The MS profile revealed the CaCO<sub>3</sub> decomposition around 600–700 °C and the volatile nature of SiO<sub>2</sub> in the form of SiO radicals at elevated temperatures (e.g. 1020 °C). The resulting powders from the HT-XRD scans in the presence of air exhibited two

visibly different layers. The top layers (in contact with air) had a grey color. The bottom layers (in contact with the sample holder) had a dark blue color. The yields of Mixture 1 (containing CaCO<sub>3</sub>) indicated a reproducible maximum in the yield around the 7 °C/min heating rate, which could imply that the CO<sub>2</sub> production is sensitive to the heating rate. No maximum was found in the yield with Mixture 2 (containing CaO). Cristobalite formation at high temperatures (e.g. 1020 °C) was not supported as a precursor to EB, nor was a trend found that cristobalite would remove a reactant through the phase transformation of quartz.

EB synthesis was attempted in  $N_2$  atmosphere, however no measurable EB was formed, which confirmed the hypothesis that  $O_2$  was needed for the synthesis, if only to prevent the formation of  $Cu^+$ . This observation also implied that  $Cu^{2+}$  ions are needed during the synthesis. Both  $CaCO_3$  and CaO were good starting constituents for the synthesis and produced similar yields of EB, however care must be taken with heating rate if  $CaCO_3$  is used as the precursor. The samples were held at  $1050~^{\circ}C$  for only 5 min instead of 16 h. Even though this gave the precursors significantly less time to react, good yields (60-70% by XRD) of EB were still obtained. The reaction time and potential uneven distribution of heat at these short times might have supported a moving boundary layer of reaction extent. Fluorescence spectroscopy confirmed the presence of optically functional 2-D layered material. SEM-EDS measurements found small crystallite features of  $1-15~\mu m$  in the morphology of the synthesized EB, previously reported in the literature.

### **Declaration of competing interest**

The authors declare that they have no known competing financial interests or personal relationships that could have appeared to influence the work reported in this paper.

## Acknowledgements

The authors appreciate financial support from the Center for Energy Systems Research at TN Tech and support from funds provided by the State of Tennessee to TN Tech in recognition of the University Carnegie Classification, R2. We would also like to acknowledge support from National Science Foundation (NSF) PREM DMR-2122169 and HRD-1924241 HBCU-RISE programs. The authors also thank Dr. Joseph J. Biernacki and Dr. Cynthia Rice for insightful discussions.

The authors thank Katrina D. Pangilinan, Dr. Luke L. Daemen, and Dr. Michelle K. Kidder for performing the TGA-MS measurements. We also appreciate the help of Dr. Wayne H. Leimer and Brian Bates for carrying out the XRD measurements, and Wayne Hawkins for the SEM-EDS measurements.

Acknowledgements for early lab work by Mahdi Mohammadizadeh, John Clark, Chris Bartol, Andrew Bays, Micah Malkowski, Carole Faircloth, Emily Lane, and Kristin Tilson.

## Appendix A. Supplementary data

Supplementary data to this article can be found online at https://doi.org/10.1016/j.jpcs.2022.110738.

## References

- S.M. Borisov, C. Würth, U. Resch-Genger, I. Klimant, New life of ancient pigments: application in high-performance optical sensing materials, Anal. Chem. 85 (2013) 9371–9377.
- [2] P. Berdahl, S.K. Boocock, G.C.-Y. Chan, S.S. Chen, R.M. Levinson, M.A. Zalich, High quantum yield of the Egyptian blue family of infrared phosphors (MCuSi4O10, M= Ca, Sr, Ba), J. Appl. Phys. 123 (2018) 193103.
- [3] G. Selvaggio, A. Chizhik, R. Nißler, D. Meyer, L. Vuong, H. Preiß, N. Herrmann, F. A. Mann, Z. Lv, T.A. Oswald, Exfoliated near infrared fluorescent silicate nanosheets for (bio) photonics, Nat. Commun. 11 (2020) 1–11.
- [4] R. Nißler, O. Bader, M. Dohmen, S.G. Walter, C. Noll, G. Selvaggio, U. Groß, S. Kruss, Remote near infrared identification of pathogens with multiplexed nanosensors, Nat. Commun. 11 (2020) 1–12.

- [5] E.A. Polo, Optical bionanosensors for neurotransmitter detection, in: Nieders "achsische Staats-Und Universit" atsbibliothek Go "ttingen, 2018.
- [6] B. Guo, Q.I. Xiao, S.h. Wang, H. Zhang, 2D layered materials: synthesis, nonlinear optical properties, and device applications, Laser Photon. Rev. 13 (2019) 1800327.
- [7] J.B. Li, H.W. Liu, T. Fu, R. Wang, X.B. Zhang, W. Tan, Recent progress in small-molecule near-IR probes for bioimaging, Trends Chem. 1 (2019) 224–234.
- [8] G. Accorsi, G. Verri, M. Bolognesi, N. Armaroli, C. Clementi, C. Miliani, A. Romani, The exceptional near-infrared luminescence properties of cuprorivaite (Egyptian blue), Chem. Commun. (2009) 3392–3394.
- [9] J. Riederer, H. Schweppe, J. Winter, R.L. Feller, R.M. Johnston-Feller, B.H. Berrie, I. Fiedler, M. Bayard, R. Newman, M. Laver, Artists' Pigments: a Handbook of Their History and Characteristics, vol. 3, 1997.
- [10] H.-G. Wiedemann, H. Berke, Chemical and physical investigations of Egyptian and Chinese blue and purple, Monuments Sites 3 (2001) 154–171.
- [11] H. Berke, The invention of blue and purple pigments in ancient times, Chem. Soc. Rev. 36 (2007) 15–30.
- [12] X.-Q. Song, M.-Q. Xie, K. Du, W.-Z. Lu, W. Lei, Synthesis, crystal structure and microwave dielectric properties of self-temperature stable Ba1-xSrxCuSi2O6 ceramics for millimeter-wave communication. J. Materiom. 5 (2019) 606–617.
- [13] G. Pozza, D. Ajo`, G. Chiari, F. De Zuane, M. Favaro, Photoluminescence of the inorganic pigments Egyptian blue, Han blue and Han purple, J. Cult. Herit. 1 (2000) 393–398.
- [14] H. Jaksch, W. Seipel, K.-L. Weiner, A. El Goresy, Egyptian blue—cuprorivaite a window to ancient Egyptian technology, Naturwissenschaften 70 (1983) 525–535.
- [15] P. Bianchetti, F. Talarico, M.G. Vigliano, M.F. Ali, Production and characterization of Egyptian blue and Egyptian green frit, J. Cult. Herit. 1 (2000) 179–188.
- [16] S. Pag`es-Camagna, S. Colinart, The Egyptian green pigment: its manufacturing process and links to Egyptian blue, Archaeometry 45 (2003) 637–658.
- [17] G.A. Mazzocchin, D. Rudello, C. Bragato, F. Agnoli, A short note on Egyptian blue, J. Cult. Herit. 5 (2004) 129–133.
- [18] T. Pradell, N. Salvado, G.D. Hatton, M.S. Tite, Physical processes involved in production of the ancient pigment, Egyptian blue, J. Am. Ceram. Soc. 89 (2006) 1476–1431
- [19] D. Johnson-McDaniel, T.T. Salguero, Exfoliation of Egyptian Blue and Han Blue, two alkali earth copper silicate-based pigments, JoVE: JoVE (2014).
- [20] D. Johnson-McDaniel, S. Comer, J.W. Kolis, T.T. Salguero, hydrothermal formation of calcium copper tetrasilicate, Chem. A Europ. J. 21 (2015) 17560–17564.
- [21] A. Panagopoulou, K. Karanasios, G. Xanthopoulou, Ancient Egyptian blue (CaCuSi4O10) pigment by modern solution combustion synthesis method, Eurasian Chemico-Technol. J. 18 (2016) 31–37.

- [22] S. Shahbazi, J.V. Goodpaster, G.D. Smith, T. Becker, S.W. Lewis, Preparation, characterization, and application of a lipophilic coated exfoliated Egyptian blue for near-infrared luminescent latent fingermark detection, Forensic Chem. 18 (2020) 100208
- [23] A. Pabst, Structures of some tetragonal sheet silicates, Acta Crystallogr. 12 (1959) 733–739
- [24] J.P. Leonard, C.B. Nolan, F. Stomeo, T. Gunnlaugsson, Photochemistry and Photophysics of Coordination Compounds: Lanthanides, Photochemistry and Photophysics of Coordination Compounds II, 2007, pp. 1–43.
- [25] S.D. Bergman, D. Gut, M. Kol, C. Sabatini, A. Barbieri, F. Barigelletti, Eilatin complexes of ruthenium and osmium. Synthesis, electrochemical behavior, and near-IR luminescence, Inorg. Chem. 44 (2005) 7943–7950.
- [26] A. Kenyon, Erbium in silicon, Semicond. Sci. Technol. 20 (2005) R65.
- [27] K. Kuriki, Y. Koike, Y. Okamoto, Plastic optical fiber lasers and amplifiers containing lanthanide complexes, Chem. Rev. 102 (2002) 2347–2356.
- [28] J.R. Weber, J.J. Felten, B. Cho, P.C. Nordine, Glass fibres of pure and erbium-or neodymium-doped yttria-alumina compositions, Nature 393 (1998) 769–771.
- [29] P. Wang, J.M. Dawes, P. Dekker, D.S. Knowles, J.A. Piper, B. Lu, Growth and evaluation of ytterbium-doped yttrium aluminum borate as a potential selfdoubling laser crystal, JOSA B 16 (1999) 63–69.
- [30] J. Fast, H. Bruning, Entkohlung und Entstickung von Eisen-Silicium-Legierungen, Zeitschrift für Elektrochemie, Ber. Bunsen Ges. Phys. Chem. 63 (1959) 765–770.
- [31] E.J. Opila, J.L. Smialek, R.C. Robinson, D.S. Fox, N.S. Jacobson, SiC recession caused by SiO2 scale volatility under combustion conditions: II, thermodynamics and gaseous-diffusion model, J. Am. Ceram. Soc. 82 (1999) 1826–1834.
- [32] T. Van De Putte, D. Loison, J. Penning, S. Claessens, Selective oxidation of a CMnSi steel during heating to 1000° C: reversible SiO 2 oxidation, Metall. Mater. Trans. 39 (2008) 2875.
- [33] R.L. Snyder, The use of reference intensity ratios in X-ray quantitative analysis, Powder Diffr. 7 (1992) 186–193.
- [34] G. Giammaria, L. Lefferts, Catalytic effect of water on calcium carbonate decomposition, J. CO2 Util. 33 (2019) 341–356.
- [35] M. del Carmen Guti errez-Castorena, W.R. Effland, Pedogenic and biogenic siliceous features, in: Interpretation of Micromorphological Features of Soils and Regoliths, Elsevier, 2010, pp. 471–496.
- [36] W.W. Schmahl, I. Swainson, M. Dove, A. Graeme-Barber, Landau free energy and order parameter behaviour of the α/β phase transition in cristobalite, Z. Kristallogr. 201 (1992) 125–145.